Renewable Energy 201 (2022) 608–623

Contents lists available at ScienceDirect

Renewable Energy

journal homepage: www.elsevier.com/locate/renene

Integrated dynamic analysis of a spar floating wind turbine with a hydraulic drivetrain

Zhiyu Jiang [a,*], Limin Yang [b], Zhen Gao [c,d,e], Torgeir Moan [c,d]

[a] Department of Engineering Sciences, University of Agder, N-4898 Grimstad, Norway
[b] DNV, Veritasveien 1, 1363, Høvik, Norway
[c] Department of Marine Technology, Norwegian University of Science and Technology (NTNU), Trondheim, Norway
[d] Centre for Autonomous Marine Operations and Systems, NTNU, Trondheim, Norway
[e] Centre for Research-based Innovation of Marine Operations, NTNU, N-7491, Trondheim, Norway

ARTICLE INFO

Keywords:
Hydraulic transmission
Spar floating wind turbine
Dynamic link library
Response dynamics

ABSTRACT

Conventional drivetrains with gearbox failures are associated with major downtime in offshore wind turbines. This impacts the maintenance cost and cost of energy. A hydraulic transmission eliminates the need for gearbox and potentially improves the turbine reliability. This paper explores the application of a novel high-pressure transmission machinery to a utility-scale spar floating wind turbine. We present a dynamic model of a hydraulic system consisting of a hydraulic pump, pipelines, a hydraulic motor, and an induction generator. The motor is placed inside the spar platform and operates at a fixed displacement. The hydraulic system is coupled with the aero-hydro-elastic code HAWC2 through an external dynamic link library. The dynamic responses of a 5 MW spar floating wind turbine and a land-based reference wind turbine with this hydraulic system were investigated under various wind and wave conditions. A comparison is made between the characteristics of the two wind turbines under operational conditions and both turbines show decent behaviors, and the statistics of power generation is at the same level compared to that of conventional wind turbines. Through simulation studies, we verify the feasibility and the engineering practice of the proposed hydraulic drive solution to floating wind turbines.

1. Introduction

Gearboxes are one of the most expensive components of a wind turbine system. Operational experience reveals that the gearboxes of modern megawatt (MW)-class electrical utility wind turbines are the weakest link among their components [1]. To address the problems and increase the reliability of gearboxes, efforts have been made to improve load prediction, design, fabrication, and operation over the past three decades [2]. In addition, the incremental development of new transmission and conversion systems has been under way. For example, the gearless, or direct-drive wind turbine concept was first proposed by the Enercon Company of Germany. This concept couples the rotor directly to a low-speed generator and reduces the number of mechanical components. It is expected to be competitive for power ratings of 4–6 MW [1]. Along with direct-drive generators, a medium-speed drivetrain system with a two-stage gearbox has also appeared on the market. This configuration may have a superior cost-of-energy performance for power ratings of approximately 6 MW or above [3]. Despite the development, the drivetrain technologies for multi-MW wind turbines still remain unproven. For offshore wind turbines, the increased cost of access to offshore wind farms necessitates less maintenance and more reliable drivetrains.

Hydraulics offers a promising drivetrain technology for wind power applications and is identified as one of the future emerging technologies in the wind power sector [4]. The main components of a hydraulic transmission system include a hydraulic pump, hydraulic pipes, and a hydraulic motor. The rotor drives the hydraulic pump, displacing fluid and creating a flow. The hydraulic fluid flows through the pipes toward the hydraulic motor. The motor converts the flow into rotation and produces power through a generator.

Hydraulic fluid has been successfully applied in many branches of engineering where large forces must be controlled in an intelligent manner [5]. For wave energy devices such as the Edinburgh duck [6] or heaving buoys [7], the wave-induced body motions are converted into electricity through hydraulic systems. Salter and Rea [5] envisaged that the components designed for wave energy converters could be used for wind power without a considerable increase in complexity. However, early testing of wind turbines with hydraulic transmission found poor

* Corresponding author.
E-mail address: zhiyu.jiang@uia.no (Z. Jiang).

https://doi.org/10.1016/j.renene.2022.10.104
Received 1 September 2022; Received in revised form 15 October 2022; Accepted 23 October 2022
Available online 30 October 2022

efficiency, primarily because of a lack of specifically designed components for hydraulic turbines in the 1980s [8]. Since then, there have been several attempts to study hydraulic wind turbine concepts [9–15]. A 1 MW test bench of a hydrostatic drivetrain was completed at Aachen University in 2010 [10]. It allows real-time simulation of different combinations of pumps and motors. The Delft Offshore Turbine transmission concept has been proposed at TU Delft. This concept utilizes seawater as the power transmission medium and uses one hydro-power-like generator station for multiple turbines [9]. Skaare et al. [13] proposed a two-speed hydraulic system based on fixed-displacement radial piston hydraulic machines. The transmission efficiency of this concept is greatly improved compared with other hydraulic transmission concepts. Mitsubishi Heavy Industries, Ltd succeeded in the development of a hydraulic transmission system with a large capacity (>7 MW) by applying digital control technology of Artemis Intelligent Power, Ltd [14]. These hydraulic concepts differ in terms of component location and functionality. The motor can be either placed in the nacelle [14] or on the ground [13]. Some configurations use variable-displacement pump and motor with synchronous generators and free of power electronics [10,14], whereas others consider fixed-displacement motors with asynchronous generators [13,16]. Today, although hydraulic transmission in wind turbines is technically feasible, it is possible to construct drivetrain prototypes with up to approximately 1 MW of nominal power output using available off-the-shelf hydraulic components [9].

Some major advantages of a hydraulic transmission system are summarized in the following [9]:

- The nacelle weight and the dimensions of support structures can be reduced.
- The elimination of the gearbox and frequency converter lowers the requirements for maintenance, and improves reliability.
- The loads are shared across many pumping modules, causing a low risk of overload and overheating.

All these points can have special economic implications for offshore wind turbines [17]. Yet, limited applications can be found to offshore wind turbines, let alone floating wind turbines. According to a comprehensive review of the hydraulic technologies in wind turbines [18], only one literature is related to floating wind turbines. Chen et al. [19] proposed a hydraulic transmission system in an offshore wind turbine with retractable blades mounted on a floating platform and tested the efficiency of the energy conversion device on a test rig. However, this study does not address any details of the floating platform or the coupled dynamics of the hydraulic system with the platform. As developments of the offshore wind industry moves from shallow to deep water in the past decade, many floating wind turbine concepts have been proposed. The spar floating wind turbine is among the most technically mature concepts [20] suitable for rough offshore environments; see [21] for full-scale measurements from the floating wind turbine Hywind Demo 1. Currently, the construction of spar floating wind farm, Hywind Tampen, is underway in the North Sea [22]. Thus, it is interesting to consider the application of novel hydraulic transmission systems to spar floating wind turbines.

The integrated analysis of the system behavior under dynamic conditions is the key to developing good designs of wind turbines. Offshore wind turbines operate under complex conditions. According to the design standards [23,24], various design situations, such as extreme environments [25] and fault scenarios [26], should be considered in the dynamic analysis. Modeling and analysis of wind turbines can be performed using aero-hydro-servo-elastic tools such as HAWC2 [27], FAST [28], or GH Bladed [29]. In most of these tools, control actions can be achieved through an externally compiled dynamic link library (DLL) whereby user-defined subroutines are executed at each time step without changing the main program. For a hydraulic turbine, the hydraulic transmission itself can be modeled in a similar manner as that used for wave energy facilities [30]. The hydraulic transmission

Fig. 1. Image of Hywind Demo, the world's first megawatt-sized floating wind turbine, located 10 km off the west coast of Norway.
Source: Equinor ASA.

subsystem, expressed as ordinary differential equations (ODEs), can also be implemented in a DLL for an aeroelastic code. Laguna [12] implemented a DLL in GH Bladed and performed a parametric study on the dynamic behavior of a hydraulic 5 MW land-based wind turbine below the rated wind speed. It was found that the amount of oil in the transmission line plays an important role on the system dynamics. Jiang et al. [31] demonstrated a numerical approach for time-domain simulations of a land-based wind turbine coupled with a hydraulic transmission system. The hydraulic ODEs were implemented in a DLL and solved using the Runge–Kutta–Fehlberg method [32]. The HAWC2 main program uses time steps on the order of 10^{-2} s, whereas solving the hydraulic ODEs requires time steps on the order of 10^{-6} s.

In this paper, we focus on the application of a hydraulic transmission system (with pumps, pipelines and motors) to a 5-MW spar floating wind turbine, and fully coupled numerical simulations were conducted under various environmental conditions of wind and waves. As the purpose of the present study is to investigate the dynamics and show feasibility of the spar hydraulic turbine under operational conditions, we also carry out simulations for a land-based wind turbine with the same hydraulic drivetrain.

2. System description

The hydraulic system and the land-based and floating wind turbine (FWT) systems are described separately in this section.

2.1. Hydraulic system

Fig. 2 shows a simplified sketch of the hydraulic system in use. The main components are a fixed-displacement radial piston hydraulic pump, a fixed-displacement axial piston motor, a variable-speed induction generator, and control valves. The hydraulic pump is placed in the nacelle, whereas the motor and generator are on the ground for the land-based wind turbine (LWT) or at the sea water level for the FWT. The configuration of the current system is similar to the one presented by [13]. Therefore, only the most relevant equations are provided here.

2.1.1. Radial piston pump

Fig. 3 illustrates a radial piston pump from Bosch Rexroth AG. A radial piston pump uses a drive shaft to drive pistons along cylinder bores to pump fluid. The back and forth motion of pistons pumps fluid

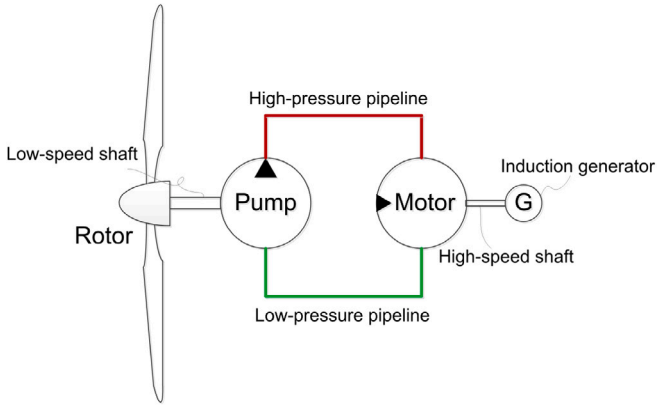

Fig. 2. Schematic of a hydraulic transmission for wind turbine.

Fig. 3. Example of a radial piston pump [33].

through the pump. This type of piston pump has a high reliability and a low noise level, making it well-suited for wind turbine applications.

The following mass balance law can be established for a volume V of liquid under isothermic conditions [34]

$$\frac{d}{dt}(\rho V) = w_{in} - w_{out} \tag{1}$$

Here, ρ is the density of the hydraulic fluid, and w_{in} and w_{out} are the mass flows into and out of the volume.

Under isothermic conditions, such a relation exists between the liquid pressure and density [34]

$$\dot{\rho} = \frac{\rho}{\beta}\dot{P} \tag{2}$$

where P is the pressure and β is the bulk modulus. Reformulating Eq. (1) using Eq. (2), we obtain the dynamic model for the high-pressure hydraulic volume of the pump

$$\frac{V_p}{\beta}\dot{P}_p + \dot{V}_p = -Q_{ip}(P_p - P_{low}) - Q_{ep}P_p - Q_p \tag{3}$$

where V_p is the volume at the high-pressure side of the pump, P_p and P_{low} are the pump pressures at the high-pressure and low-pressure side, respectively. Q_{ip} is the coefficient for internal leakage, and Q_{ep} is the coefficient for external leakage. Q_p is the outlet flow rate from the pump. The hydraulic fluid at the high-pressure side is compressed because of the motion of the pistons. Therefore, $\dot{V}_p$, the time derivative of V_p, can be expressed as

$$\dot{V}_p = -D_p\omega_p \tag{4}$$

where D_p is the pump displacement, and ω_p is the pump speed. Assuming that the low-speed shaft is rigid, ω_p can be replaced by the rotor speed ω_t. From Eq. (3), we obtain

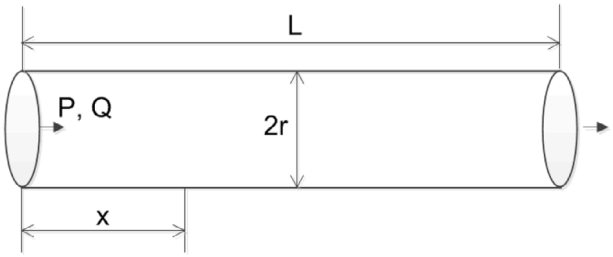

Fig. 4. Illustration of a fluid transmission line.

$$\dot{P}_p = \frac{\beta}{V_p}[\omega_t D_p - Q_{ip}(P_p - P_{low}) - Q_{ep}P_p - Q_p] \tag{5}$$

For the pump shaft, Newton's second law holds, and the following dynamic model is found

$$J_p\dot{\omega}_t = \eta T_t - C_p\omega_p - D_p(P_p - P_{low}) \tag{6}$$

where J_p represents the moment of inertia of the hydraulic pump, η is the mechanical efficiency, T_t is the shaft torque, and C_p is the viscous damping coefficient. We neglect the viscous damping (C_p=0), assume ideal efficiency (η=1), and simplify the expression of the shaft torque as

$$T_t = J_p\dot{\omega}_t + D_p(P_p - P_{low}) \tag{7}$$

2.1.2. Transmission line

The dynamics of the hydraulic transmission line are important for the analysis. The pipelines extend from the nacelle level to the tower base. Because of the length, there is spatial variation in the pressure, and because it takes time for the pressure to propagate, the time delay between the aerodynamic power and the development of hydraulic power may be relevant for the control system design [13].

Fig. 4 shows a single transmission line with length L and inner radius r. The length coordinate along the pipe is denoted by x. P and Q are the fluid pressure and flow rate, respectively; they are functions of x and t. The dynamic model of the pressure wave propagation in the transmission line is found from the principle of mass and momentum balance [34]. Assuming that the pipeline is rigid and that the flow is laminar, the pressure wave propagation can be described by two one-dimensional partial differential equations

$$\frac{\partial P(x,t)}{\partial t} + \frac{\rho a^2}{A_{pipe}}\frac{\partial Q(x,t)}{\partial x} = \frac{\rho a^2}{A_{pipe}}S_Q(x,t) \tag{8}$$

$$\frac{\partial Q(x,t)}{\partial t} + \frac{A_{pipe}}{\rho}\frac{\partial P(x,t)}{\partial x} = \frac{F(x,t)}{\rho} \tag{9}$$

where A_{pipe} is the cross sectional area of the pipe, ρ is the fluid density, a is the acoustic velocity, $F(x,t)$ is any externally applied force per length, and $S_Q(x,t)$ represents the volume flow into the pipe per length. To find time-domain solutions to Eqs. (8)–(9), different approaches can be used, such as the rational transfer function (RTF) method and the separation of variables technique [35].

In this work, the RTF method was used to construct the bond graph representations for the pipelines, considering the two-dimensional frequency-dependent friction [36]. By doing so, the hydraulic pipeline models can be represented as a number of normal modes. Only the first- and second-order modes are used here:

$$\begin{bmatrix} \dot{Q}_{p0} \\ \dot{Q}_{m0} \end{bmatrix} = \omega_c \left[\boldsymbol{A_0} \begin{bmatrix} Q_{p0} \\ Q_{m0} \end{bmatrix} + \boldsymbol{B_0} \begin{bmatrix} P_p \\ P_m \end{bmatrix} \right] \tag{10}$$

$$\begin{bmatrix} \dot{Q}_{p1} \\ \dot{Q}_{m1} \end{bmatrix} = \omega_c \left[\boldsymbol{A_1} \begin{bmatrix} Q_{p1} \\ Q_{m1} \end{bmatrix} + \boldsymbol{B_1} \begin{bmatrix} P_p \\ P_m \end{bmatrix} \right] \tag{11}$$

Using the dissipative friction model, the coefficient matrices are given by

$$\boldsymbol{A_0} = \begin{bmatrix} -8 & 0 \\ 0 & -8 \end{bmatrix},\ \boldsymbol{B_0} = \frac{1}{Z_0 D_n}\begin{bmatrix} 1 & -1 \\ 1 & -1 \end{bmatrix},\ \boldsymbol{A_1} = \begin{bmatrix} 0 & \frac{-\omega_1^2}{D_n^2} \\ 1 & -\frac{\epsilon_1}{D_n} \end{bmatrix},\ \boldsymbol{B_1} = \frac{2}{Z_0 D_n}\begin{bmatrix} 0 & 0 \\ 1 & 1 \end{bmatrix} \tag{12}$$

where the viscosity frequency ω_c, dissipation number D_n, line impedance constant Z_0, modal natural frequency ω_1, and damping coefficient ϵ_1, are defined, respectively, as follows:

$$\omega_c = \frac{\nu_0}{r^2},\ D_n = \frac{L_{pipe}\nu_0}{ar^2},\ Z_0 = \frac{\rho a}{A_{pipe}},\ \omega_1 = \pi - \frac{1}{2}\sqrt{2\pi D_n} + \frac{1}{2}D_n,\ \epsilon_1 = \sqrt{2\pi D_n} + \frac{5}{2}D_n \tag{13}$$

where ν_0 is the fluid viscous coefficient, r_{pipe} and L_{pipe} are the radius and length of the pipe, respectively.

Thus, the flow rates at the two ends of the pipeline can be found using the two normal modes as follows:

$$Q_p = Q_{p0} + Q_{m1} \tag{14}$$

$$Q_m = Q_{m0} - Q_{m1} \tag{15}$$

2.1.3. Axial piston motor

In contrast to a pump, a hydraulic motor converts pressure into torque. An axial piston motor is used in the current system. It has a number of pistons arranged in a circular array within a housing that is commonly referred to as a cylinder block. The pressure force from the pistons is transferred to the angle swashed plate lubricated slippers that are mounted onto the pistons with a ball coupling. The rotation of the cylinder block causes the pistons to oscillate in their cylinders by the action of the swash plate, which provides the conversion between the piston pressure force and the shaft torque.

The dynamic model of the hydraulic motor can be derived based on the volume balance form, similar to that of the hydraulic pump model. The output shaft is connected to the generator. Thus, the time derivative of the hydraulic volume can be represented as

$$\dot{V}_m = D_m\omega_m = D_m\omega_g \tag{16}$$

where D_m is the motor displacement and ω_m and ω_g are the motor and generator speeds. Therefore, the time derivative of the motor pressure can be written as

$$\dot{P}_m = \frac{\beta}{V_m}[Q_m - Q_{im}(P_m - P_{low}) - Q_{em}P_m - D_m\omega_g] \tag{17}$$

2.1.4. Check valves

Check valves are used to control the direction of the fluid flow. The volume flow q_v can be calculated using the orifice equation derived from Bernoulli's energy equation for an incompressible flow

$$q_v = \begin{cases} C_d A_v\sqrt{\frac{2}{\rho}(P_p - P_m)}, & \text{if } P_p > P_m \\ 0, & \text{if } P_p \le P_m \end{cases} \tag{18}$$

where C_d is the discharged coefficient and A_v is the cross sectional area of the valves.

2.1.5. Variable-speed generator

The generator torque-versus-speed curve for the NREL 5 MW turbine is used in the current paper. As shown in Fig. 5, the curve contains five control regions: Region 1 is a control region before the cut-in wind speed; Region 2 is a control region for optimizing power capture; Region 3 has a constant generated power; Region $1_{1/2}$ is a linear transition between Regions 1 and 2; and Region $2_{1/2}$ is a linear transition between Region 2 and 3 with a torque slope corresponding to the slope

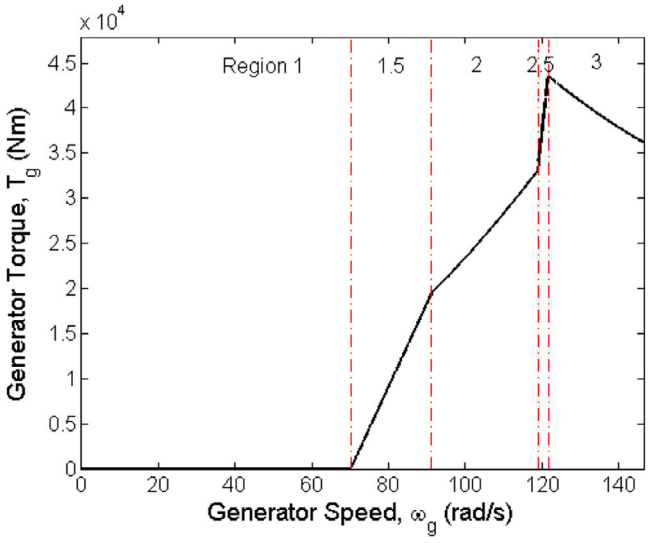

Fig. 5. Torque–speed relation of the variable-speed generator controller [37].

of an induction machine. The generator-slip percentage in the transition region $2_{1/2}$ is 10%. Additional details can be found in [37].

The shaft of the hydraulic motor is connected to the electric generator, and the state equation defining the coupling between the motor and the generator can be expressed as

$$(J_m + J_g)\dot{\omega}_g = D_m P_m - C_m\omega_g - T_g \tag{19}$$

where J_m and J_g are the moment of inertia of the motors and generator, ω_g is the generator speed, D_m is the displacement of the motors, C_m is the viscous damping of the motor-generator shaft, and T_g is the generator torque.

2.1.6. State-space model of the hydraulic system

Incorporating the subsystem models presented in Sections 2.1.1–2.1.5, we can develop a complete dynamic model for the hydraulic system. The state variables are defined as $y = [P_p, \dot{P}_m, \dot{Q}_{p0}, \dot{Q}_{p1}, \dot{Q}_{m0}, \dot{Q}_{m1}, \dot{\omega}_g]^T$. A set of constant parameters used for the analysis is summarized in Table 1. Values for the hydraulic pump and motor can be found in [13]. The estimated leakage coefficients may be updated if other case-specific data are available. For the hydraulic system and in the coupled analysis, the input variable is ω_t, and the output to the aeroelastic code is T_t.

2.2. Land-based and floating wind turbines

This study selects the NREL 5 MW LWT [37] and the OC3 Hywind spar FWT [38] as two representative examples. A schematic of the FWT with hydraulic components is illustrated in Fig. 6. As shown, the motor and generator are placed on the deck level. For the LWT, these components are on the ground level.

According to the analysis with HAWC2, the first and second full-system natural frequencies of the LWT are 0.32 Hz, corresponding to the fore-aft and side-side bending mode of the tower. The spar FWT is ballast stabilized and has three sets of catenary mooring lines for station keeping purposes. The natural frequencies of the translational motions in surge, sway, and heave are 0.050, 0.050, and 0.203 rad/s, respectively. For the angular motions in pitch, roll, and yaw, the natural frequencies are 0.209, 0.209, and 0.785 rad/s, respectively.

Both turbines are variable-speed machines with generator torque control and collective blade pitch control. For the hydraulic wind turbines, the effect of the generator torque control is transferred to the main shaft (low-speed side) through the hydraulic system, and

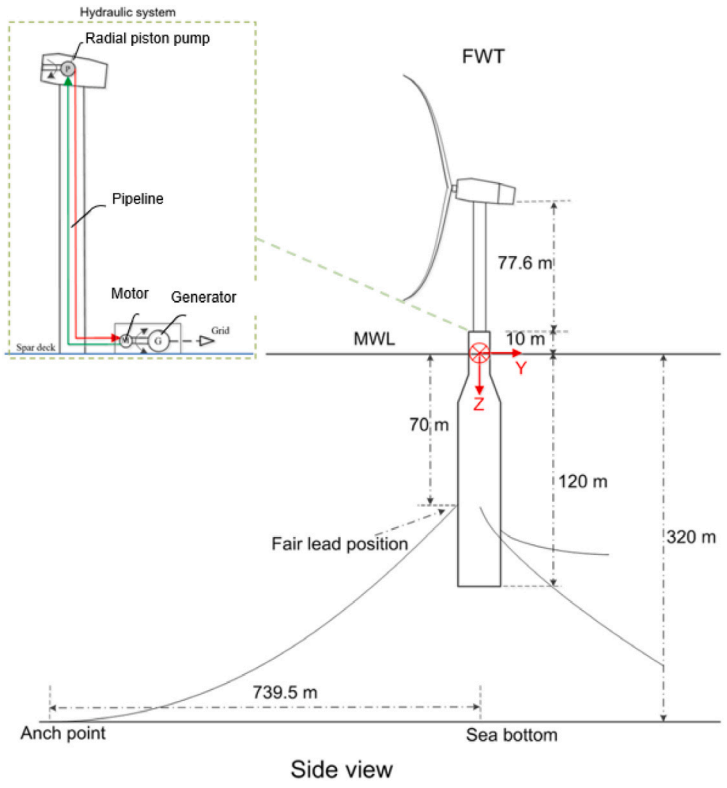

Fig. 6. Schematic of the floating wind turbine with the considered hydraulic system.

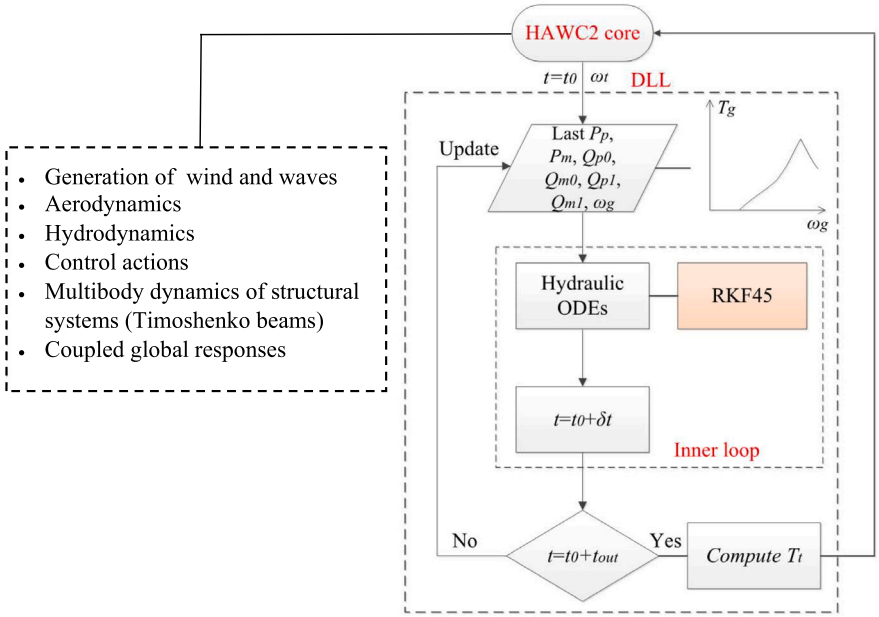

Fig. 7. Flowchart of the hydraulic module in DLL.

the computed main-shaft torque (T_t) contains dynamic effects of the hydraulic system. Assuming that the main-shaft speed can still be measured, the blade-pitch control strategy remains unchanged. Compared with the LWT, the spar wind turbine has a reduced controller-response natural frequency of 0.2 rad/s to eliminate the potential for an unstable feedback loop at the platform-pitch natural frequency [39]. Above the rated wind speed, the generator control of the floating system adopts the constant-torque strategy instead of the constant-power strategy, aiming to minimize the drivetrain loads and to reduce blade-pitch activity.

The traditional gearbox is often simplified as a one degree-of-freedom (DOF) system in aeroelastic models considering the torsional DOF only. In this work, the structural models of the hydraulic turbines resemble those of the geared turbines.

3. Numerical model

Numerical simulations were performed using the aeroelastic code HAWC2 [27]. The structural model in HAWC2 is based on multibody dynamics. Both the LWT and FWT were modeled using bodies consisting of Timoshenko beam elements. A DLL provides an interface for

Table 1
Parameters of the hydraulic transmission system.

Variable	Description	Value
J_p	Moment of inertia of hydraulic pump	5140 kg m^2
J_m	Moment of inertia of hydraulic motor	138 kg m^2
D_p	Displacement of hydraulic pump	0.2 m^3 rad^{-1}
D_m	Displacement of hydraulic motor	$2.06 \cdot 10^{-3}$ m^3 rad^{-1}
V_{2p}	Pump volume on the high-pressure side	0.045 m^3
V_{1m}	Motor volume on the high-pressure side	0.01 m^3
P_{low}	Standard atmospheric pressure	$1.0 \cdot 10^5$ Pa
Q_{ip}	Coefficient for internal pump leakage	$1.12 \cdot 10^{-10}$ Pa s^{-1}
Q_{ep}	Coefficient for external pump leakage	$5.6 \cdot 10^{-11}$ Pa s^{-1}
Q_{im}	Coefficient for internal motor leakage	$9.1 \cdot 10^{-11}$ Pa s^{-1}
Q_{em}	Coefficient for external motor leakage	$4.6 \cdot 10^{-11}$ Pa s^{-1}
r_{pipe}	Radius of the transmission line	0.14 m
L_{pipe}	Length of the transmission line	100 m
ρ	Density of the fluid	865 kg m^{-3}
ν	Kinematic viscosity coefficient of the fluid	$6 \cdot 10^{-5}$ m^2/s
β	Bulk modulus of the fluid	$1.0 \cdot 10^9$ Pa
c_{fluid}	Acoustic velocity in the fluid	1075.2 m/s
C_p	Viscous damping coefficient of pump shaft	0 N m s rad^{-1}
C_m	Viscous damping coefficient of motor shaft	0 N m s rad^{-1}

specifying external loading or control actions. In addition to the blade pitch control, we implemented the state-space model of the hydraulic system in the DLL. For the FWT, the mooring and wave forces were implemented as force elements using the DLL. Wave loads normal to the spar floater were calculated using Morison's equation [40], while the buoyancy forces and heave excitation on the floater were considered using a simplified pressure integration method including the hydrostatic and hydrodynamic pressures, respectively [41].

We focus our discussion on the part of the DLL that addresses the hydraulic system here. There is a data exchange between the hydraulic module and the HAWC2 core during the time-domain simulation. As shown in Fig. 7, each time the HAWC2 core calls the DLL, the rotor speed, ω_t, is passed to the DLL and an initial value problem must be solved through the hydraulic ODEs (Eqs. (5), (7), (10), (11), and (19)). The Runge–Kutta–Fehlberg (RKF45) method [32,42] is employed to address the problem. Inside an inner loop, the RKF45 routine adjusts its "locally optimal" step sizes on the order of 10^{-6} s and returns the fifth-order solution approximation at $t_0 + \delta t$. Each inner loop finishes when the user-specified step length δt is reached. Here, t_{out} represents the time interval in HAWC2 (0.02 s). When t_{out} is reached, the DLL transfers the main-shaft torque T_t to the main program [31].

From the coupled dynamic simulations in the time domain, global responses of the floater motions, structural deformations, sectional forces and moments, and power performances are available. In addition, the DLL outputs response variables of the hydraulic system, e.g., pipeline fluid pressure and motor displacements, at each time step. This makes it possible to study the response dynamics of the whole hydraulic wind turbine systems.

4. Environmental conditions

The environmental conditions (ECs) used in this study are summarized in Table 2. Because we consider the design situation of normal operation, the wind speed in ECs 1–7 spans various control regions of the wind turbines during power production. For the design and analysis of FWTs, realistic combinations of wind and waves are recommended. Li et al. [43] analyzed five European offshore sites and obtained the long-term joint distributions of the 1-hour mean wind speed at the 10-m level (U_w), significant wave height (H_s) and spectral peak period (T_p) using the hindcast data.

Among the five sites, we select the one in the northern North Sea (Table 3) for the FWT. This site has a water depth of over 200 m and can be considered for the deployment of FWTs. The theoretical expected values of H_s and T_p were calculated for a given hub-height wind speed (U_{hub}), using the relations developed in [43]. A power law with an exponent of α=0.14 was applied to scale the wind speed at the hub height to the wind speed at the 10-m height. For the FWT, wind and waves were assumed to be aligned in the y direction (Fig. 6).

In Table 2, TI stands for turbulence intensity. For the normal turbulence model, TI is given by

$$TI = \frac{I_{ref}(0.75U_{hub} + 5.6)}{U_{hub}} \tag{20}$$

where I_{ref} equals 0.16, 0.14, and 0.12 for wind turbine class (WTC) A, B, and C, respectively [23]. WTC C has low turbulence characteristics and is dedicated to offshore wind turbines. As shown, three turbulence levels are considered for both turbines: zero turbulence, higher turbulence characteristics, and lower turbulence characteristics. The Mann uniform shear turbulence model was used to generate the turbulent wind field.

Each simulation lasts 800 s, among which the first 200 s are removed in the analysis to avoid start-up transients. For the LWT in the turbulent wind cases and for the FWT in all cases, 20 simulations with random seed numbers were conducted to reduce the statistical uncertainties in the time-domain simulations.

5. Results and discussion

In this section, the simulation results of the turbine models incorporating the hydraulic system are presented. The statistical data of the turbulent cases are based on an average of 20 simulations. The results do not include the mechanical efficiency of the pump or motor. Neither the efficiency of the generator nor that of the power electronics was included when calculating the generator power.

5.1. Land-based wind turbine

Figs. 8–9 show the time series of the hydraulic turbine at representative wind speeds under constant and turbulent wind conditions. The turbulent-wind cases shown have high turbulence levels, corresponding to WTC A. Therefore, the hub-height wind speed varies significantly around the mean value. The numerical simulations are stable both below and above the rated wind speed. The hydraulic torque, T_t is connected at 150 s in the simulations, but only the part from 200 s is presented in the figures. Under constant wind conditions, all response variables approach constant values soon after the connection of the hydraulic torque, indicating that the current hydraulic system is suitable for the turbine system. As shown in Fig. 9(a), the flow rate through the hydraulic pump reaches approximately 0.25 m^3/s, and the corresponding pump pressure is 209 bar. The ratios between the main-shaft torque and the generator torque are 95.1, 96.1, 96.4, 96.6, 96.6, 96.6 and 96.6 at constant wind speeds of 6, 8, 10, 11.4, 14, 18 and 22 m/s. Because the torque–speed relation of the generator remains the same as the one for the NREL 5 MW baseline turbine, these values are close to the original gear ratio of 97. If other generator characteristics are applied, we may observe different ratios.

At U_{hub}=8 m/s, the blade pitch angle is zero, and a constant rotor speed is only reached by balancing T_t with the external aerodynamic torque. At U_{hub}=18 m/s, the average blade pitch angle increases to approximately 13.7° to limit the power. The effective blade pitch control above the rated wind speed reduces the fluctuations in all investigated variables except the main-shaft torque, which also has large fluctuations at U_{hub}=18 m/s. Above the rated wind speed, the external aerodynamic torque still experiences large variations because of the turbulence, and the main-shaft torque provided by the hydraulic system must vary accordingly to counteract the aerodynamic torque.

Table 2
Environmental conditions for the wind turbines.

EC	FWT				LWT	
	U_{hub} (m/s)	H_s (m)	T_p (s)	TI	U_{hub} (m/s)	TI
1	6.0	1.91	11.74	0, 0.2, 0.27	6.0	0, 0.2, 0.27
2	8.0	2.11	11.45	0, 0.17, 0.23	8.0	0, 0.17, 0.23
3	10.0	2.36	11.23	0, 0.16, 0.21	10.0	0, 0.16, 0.21
4	11.4	2.57	11.12	0, 0.15, 0.2	11.4	0, 0.15, 0.2
5	14.0	3.00	10.99	0, 0.14, 0.18	14.0	0, 0.14, 0.18
6	18.0	3.80	10.97	0, 0.13, 0.17	18.0	0, 0.13, 0.17
7	22.0	4.77	11.10	0, 0.12, 0.16	22.0	0, 0.12, 0.16

Table 3
General information about the selected European offshore site [43].

Site	No.	Area name	Geo-coordinates	Water depth (m)	Distance to shore (km)
14	North Sea	Norway 5	61.85N, 4.23E	202	30

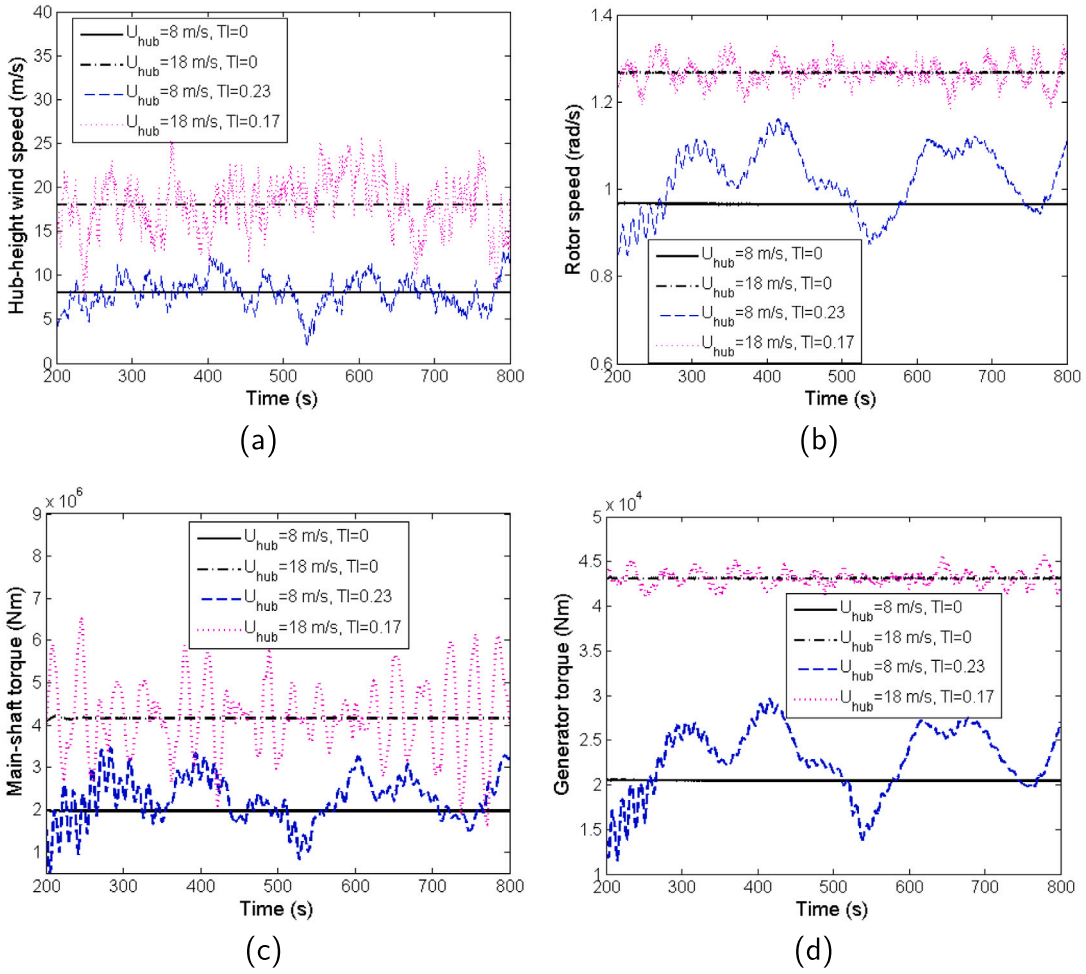

Fig. 8. Response time series of the land-based wind turbine under various wind conditions: (a) wind speed, (b) rotor speed, (c) shaft torque, and (d) generator torque.

The irregular variations in the responses (Figs. 8(c)–8(d)) of a hydraulic wind turbine are expected under turbulent wind conditions, as observed in [13]. Consequently, the rotor speed has limited accelerations, and the generator power has comparatively small deviations from the steady-state values.

Fig. 10 compares the mean values of the responses under various wind conditions. Wind turbulence does not appear to affect the mean values in most responses below or above the rated wind speed. However, compared to constant wind conditions, the high and low turbulence levels tend to increase the average blade pitch angle near the rated wind speed of U_{hub}=11.4 m/s, reducing the generator power by approximately 8% and 6% in WTC C and WTC A, respectively. As shown in Fig. 10(b), the thrust also has an appreciable decrease near the rated wind speed when the condition is changed from constant to turbulent wind. WTC A causes the lowest peak in the thrust. In contrast, the effect of the turbulent wind on the mean values of the generator speed and the pump flow rate falls below 1% across the wind speeds.

Table 4 presents the response statistics under selected wind conditions, each value calculated based on an average of twenty 600-second simulations. As shown, at U_{hub}=8 m/s, the standard deviations of variables other than the blade pitch angle exceed those at U_{hub}=18 m/s. For the generator power, the standard deviation under the condition

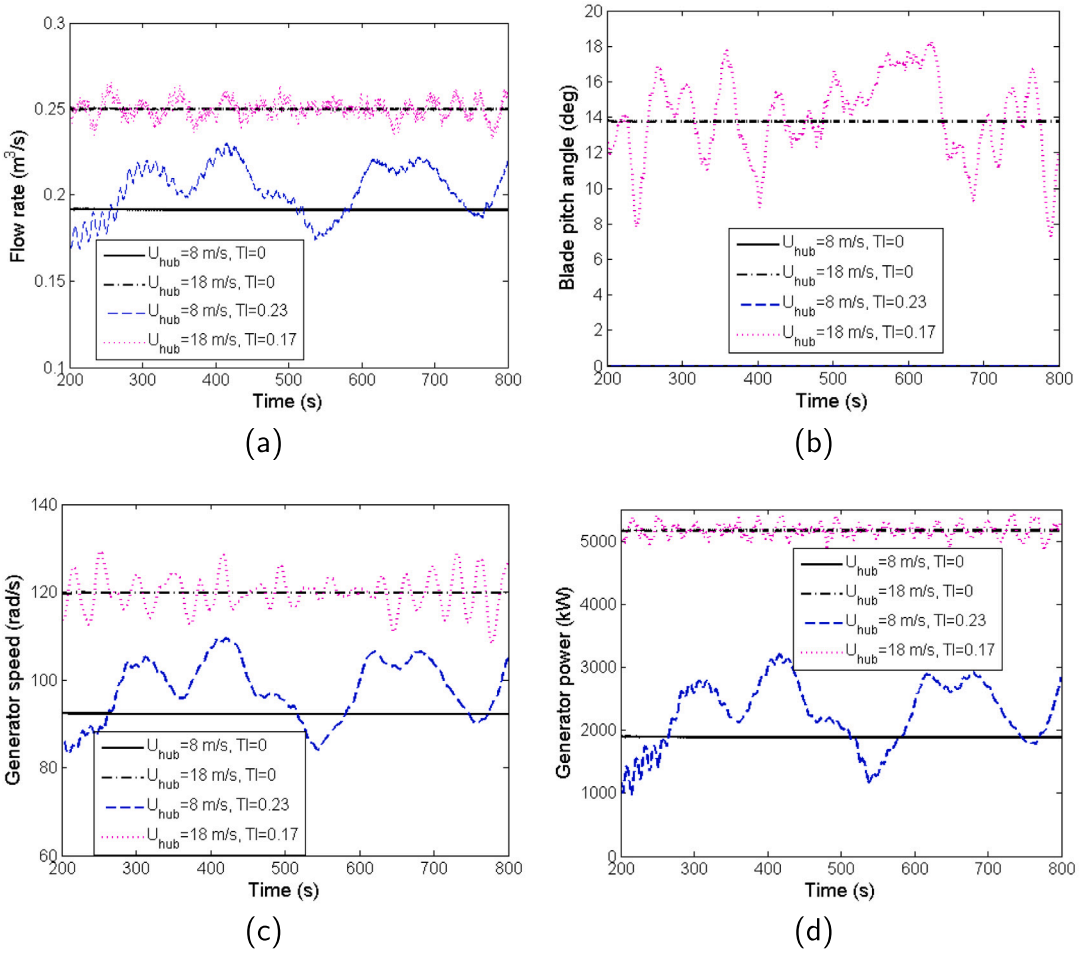

Fig. 9. Response time series of the land-based wind turbine under various wind conditions: (a) pump flow rate, (b) collective blade pitch, (c) generator speed, and (d) generator power.

of WTC A and U_{hub}=8 m/s amounts to approximately 35% of the mean power. When U_{hub} is increased to 18 m/s, the standard deviation is reduced to approximately 2% of the mean power. The standard deviation of the pump flow rate is also limited when the wind speed is above the rated speed, varying between 1%–3% of the mean value. The pump pressure experiences relatively wider range of variation, and the standard deviation can exceed 20% of the mean value. We find that larger standard deviations are always associated with higher turbulence intensities in the wind. When the wind turbulence rises from WTC C to WTC A, the average increase in the standard deviation of the thrust, rotor speed, pump flow rate and tower-bottom fore-aft bending moment lies between 26%–29% across different mean wind speeds; for the generator torque, generator speed, pump pressure and generator power, the increase can exceed 30%. Stronger wind turbulence is also connected to larger response maxima and to smaller minima. We focus on the maxima here. When the wind condition is changed from WTC C to WTC A, the maxima of the thrust and tower-bottom bending moment increase by approximately 10%. These responses are directly affected by aerodynamic excitation, and the increases have small differences between the below-rated and above-rated wind speeds. The generator power, rotor speed, generator speed, and pump flow rate are influenced by the blade pitch control above the rated wind speed. The average increase in the maxima of the rotor speed, generator speed, and pump flow rate below the rated wind speed is between 3%–4%, but for the generator power and pump pressure, the average increase ranges from 16%–19%.

5.2. Floating wind turbine

With the identical hydraulic system but with a different control strategy, the spar FWT displays interesting response characteristics during operation. Figs. 11–12 demonstrate one realization of the response time series at the rated wind speed. Here, we discuss the responses under constant and turbulent wind conditions in sequence.

Under constant wind conditions, although the wind speed from the field remains fixed, there is still a variation in the incoming wind on the rotor because of the platform motions induced by irregular waves. Therefore, unlike the LWT, the FWT does not have steady-state responses, and the rotor speed and main-shaft torque appear to have more fluctuations when the wave elevation is high. The generator speed varies within an average range of +3.10% to −3.95% of the mean generator speed in response to the constant wind speeds. This small amount of variation propagates to the generator torque and causes more fluctuation in the generator power. As shown in Fig. 12(a), the pump flow rate is comparatively stable at U_{hub}=11.4 m/s and TI=0, the maximum and minimum being within 8% of the mean value. The blade pitch angle fluctuates around a mean angle of 1.54°, with the maximum obtaining 3.8° in this simulation, indicating the minor degree of velocity excursion caused by the platform motion. Because the wave direction is aligned with the wind direction, the platform-roll motion is very limited under constant wind conditions. The platform-pitch motion varies around a positive mean, corresponding to the clockwise rotation about the x-axis in Fig. 6. This positive mean arises

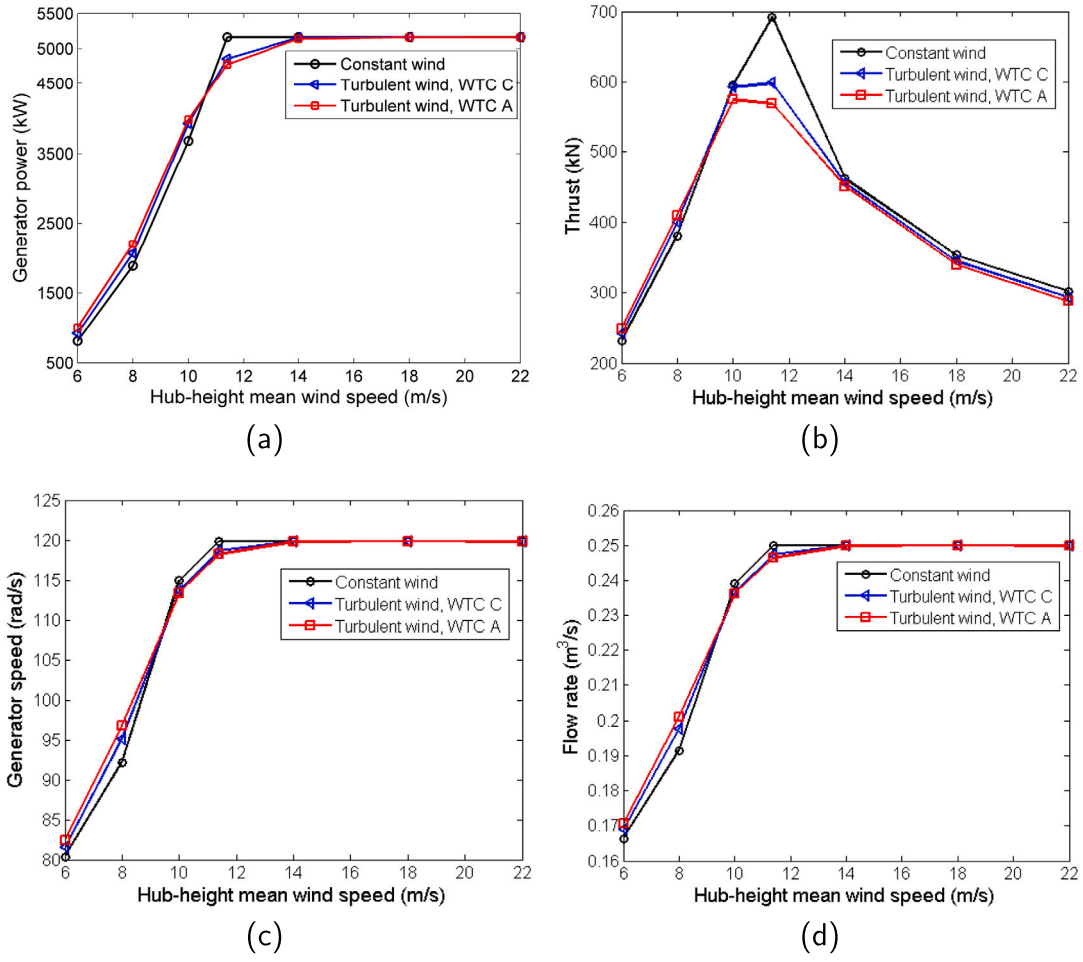

Fig. 10. Statistical means of the land-based wind turbine in ECs 1–5 (each point is obtained by averaging 20 simulations): (a) generator power, (b) thrust, (c) generator speed, and (d) flow rate.

Table 4
Response statistics under turbulent wind conditions, LWT (each value based on an average of 20 simulations).

Variable	EC	Std		Max		Min	
		WTC A	WTC C	WTC A	WTC C	WTC A	WTC C
Generator power (kW)	2	694.2	499.4	4171.6	3250.9	915.4	1085.3
	6	106.6	82.0	5474.7	5404.3	4851.9	4922.6
Generator torque (kN m)	2	5170.4	3769.8	36445.1	29799.0	10887.0	12743.4
	6	871.6	668.3	45686.3	45055.2	40746.4	41262.8
Thrust (kN)	2	99.3	74.1	694.6	602.9	188.0	229.8
	6	93.3	71.2	694.0	602.6	63.1	129.0
Rotor speed (rad/s)	2	0.09	0.07	1.23	1.16	0.84	0.86
	6	0.03	0.02	1.35	1.33	1.18	1.20
Generator speed (rad/s)	2	8.55	6.57	114.95	109.56	81.97	83.70
	6	3.73	2.87	129.52	127.30	110.27	112.44
Blade pitch angle (deg)	2	0.04	0	0.67	0	0	0
	6	2.67	2.03	19.41	18.18	6.37	8.47
Pump flow rate (m^3/s)	2	0.018	0.014	0.242	0.229	0.168	0.172
	6	0.005	0.004	0.267	0.263	0.233	0.237
Pump pressure (bar)	2	32.36	23.77	198.75	168.01	34.60	48.66
	6	42.21	32.56	319.98	294.23	99.57	124.75
Tower-base Mx (kN m)	2	10017.4	7465.2	65050.3	56094.0	6961.4	13416.46
	6	9812.6	7478.6	69900.2	60139.7	997.6	8418.9

primarily from the rotor thrust and reaches a maximum at approximately the rated wind speed. The platform-surge motion is subjected to the combined effects of wave loads, mooring line tension, and rotor thrust. In addition to the positive mean, the surge natural period can be clearly observed in the cyclic variations. There are approximately four surge cycles in the time series.

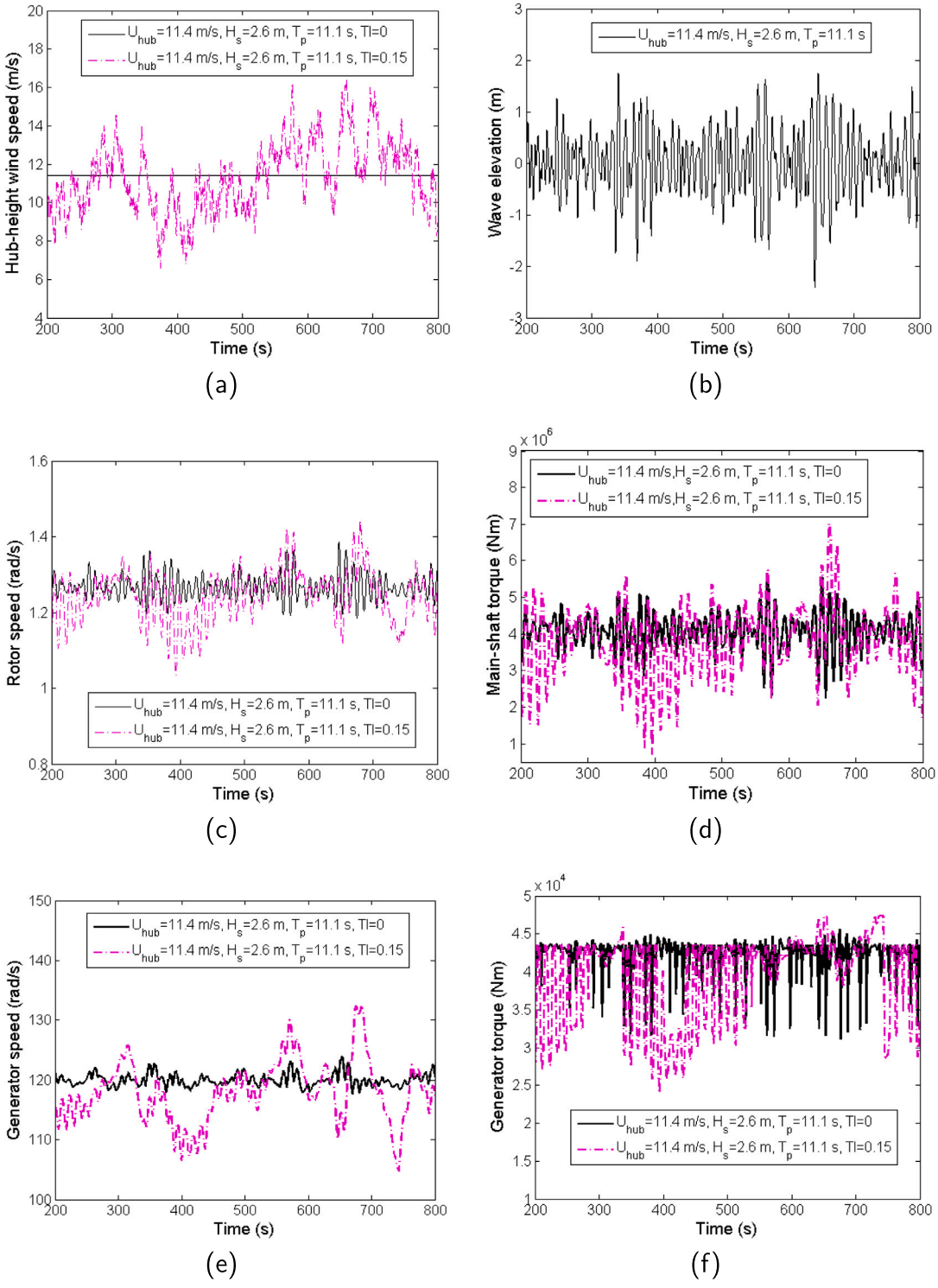

Fig. 11. Response time series of the floating wind turbine at the rated wind speed and under an irregular wave condition (EC4): (a) wind speed, (b) wave elevation, (c) rotor speed, (d) shaft torque, (e) generator speed, and (f) generator torque.

As presented in Fig. 11(a), under a turbulent wind condition with TI corresponding to WTC A, the hub-height wind speed frequently crosses the solid line during the simulation time, calling for active blade pitch control. Motion of the spar platform increases the variation in the wind loads on the rotor, and the response variables in turbulent wind have considerable variations. In Fig. 11(c), the varying rotor speed trend follows that of the hub-height wind speed. Because of the reduced controller frequency, the blade pitch controller of the FWT becomes less respondent to the rotor overspeed. At approximately 680 s, the maximum rotor speed reaches 1.4 rad/s, approximately 10% larger than the rated rotor speed. Consequently, a large generator speed also appears at this moment. The flow rate in the hydraulic pump has an evident drop when the wind speed is in the below-rated region from approximately 350 to 500 s (Fig. 12(a)). Because the hydraulic

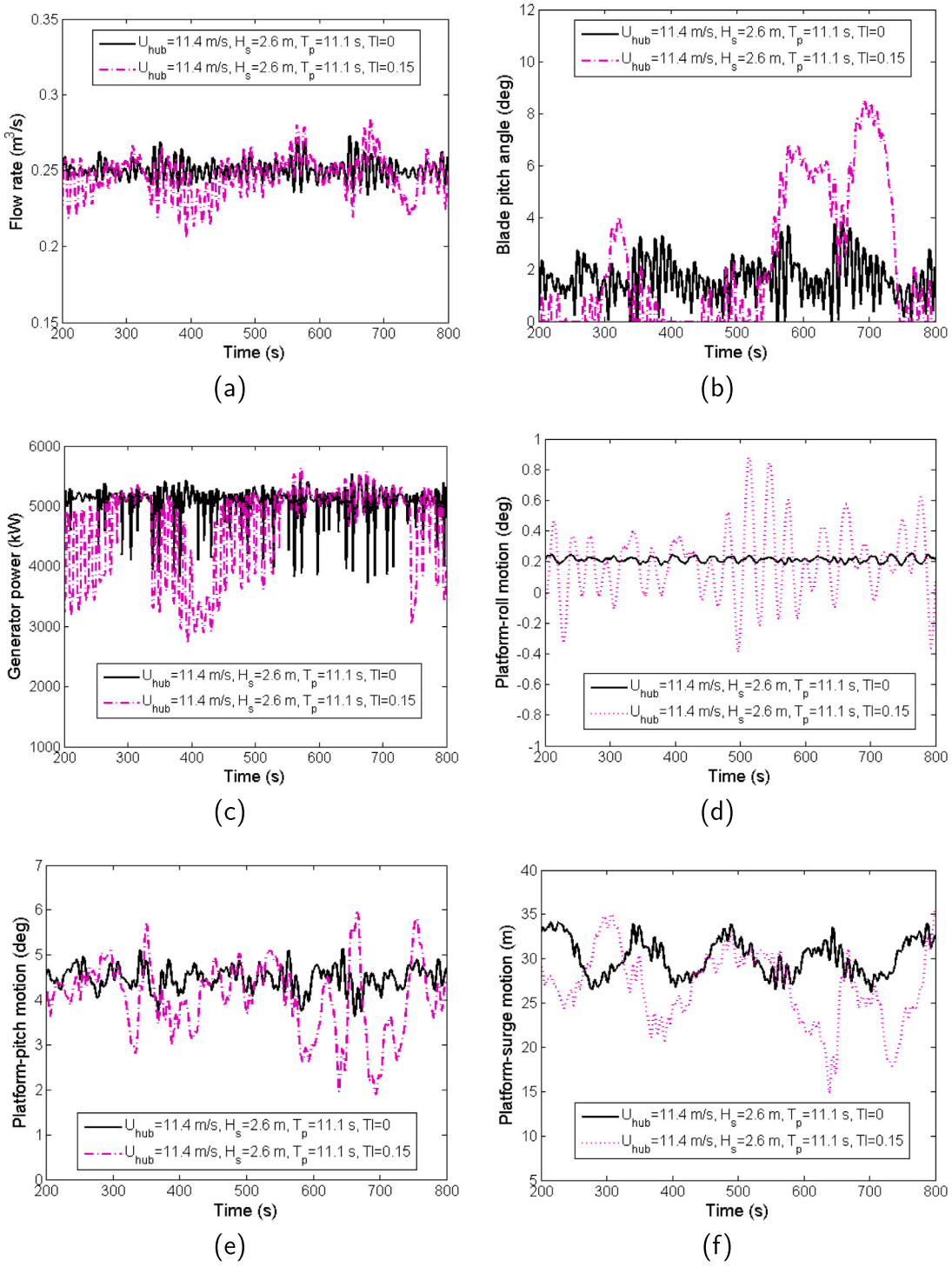

Fig. 12. Response time series of the floating wind turbine at the rated wind speed and under an irregular wave condition (EC4): (a) flow rate, (b) collective blade pitch, (c) generator power, (d) platform-roll motion, (e) platform-pitch motion, and (f) platform-surge motion.

system acts as the medium that transfers energy from the rotor side to the generator side, the dynamics of the pump pressure and flow rate are easily affected by a change in external loads. The dash dotted line in Fig. 12(b) illustrates the variation in the blade pitch angle under turbulent wind conditions. Near 700 s, the maximum pitch angle exceeds 8° in response to the rotor overspeed. Compared with the LWT, the FWT has larger fluctuations and reduced power quality. There is an evident increase in oscillations in platform-roll, -pitch, and -surge motions under turbulent wind conditions compared to under constant wind conditions, as shown in Figs. 12(d)–12(f). For roll motion, the dominant roll natural period can be clearly observed. Comparing the platform-pitch motion responses under the two wind conditions, we find that under the turbulent wind condition, the platform pitch still varies at approximately a positive mean value of 4°, but the fluctuation appears to be more significant between 620 and 780 s. This observation is primarily due to the increase in blade pitch angle during this period. The rotor thrust contributes considerably to the platform pitch, and a large increase in blade pitch angle causes a reduction in the thrust at the

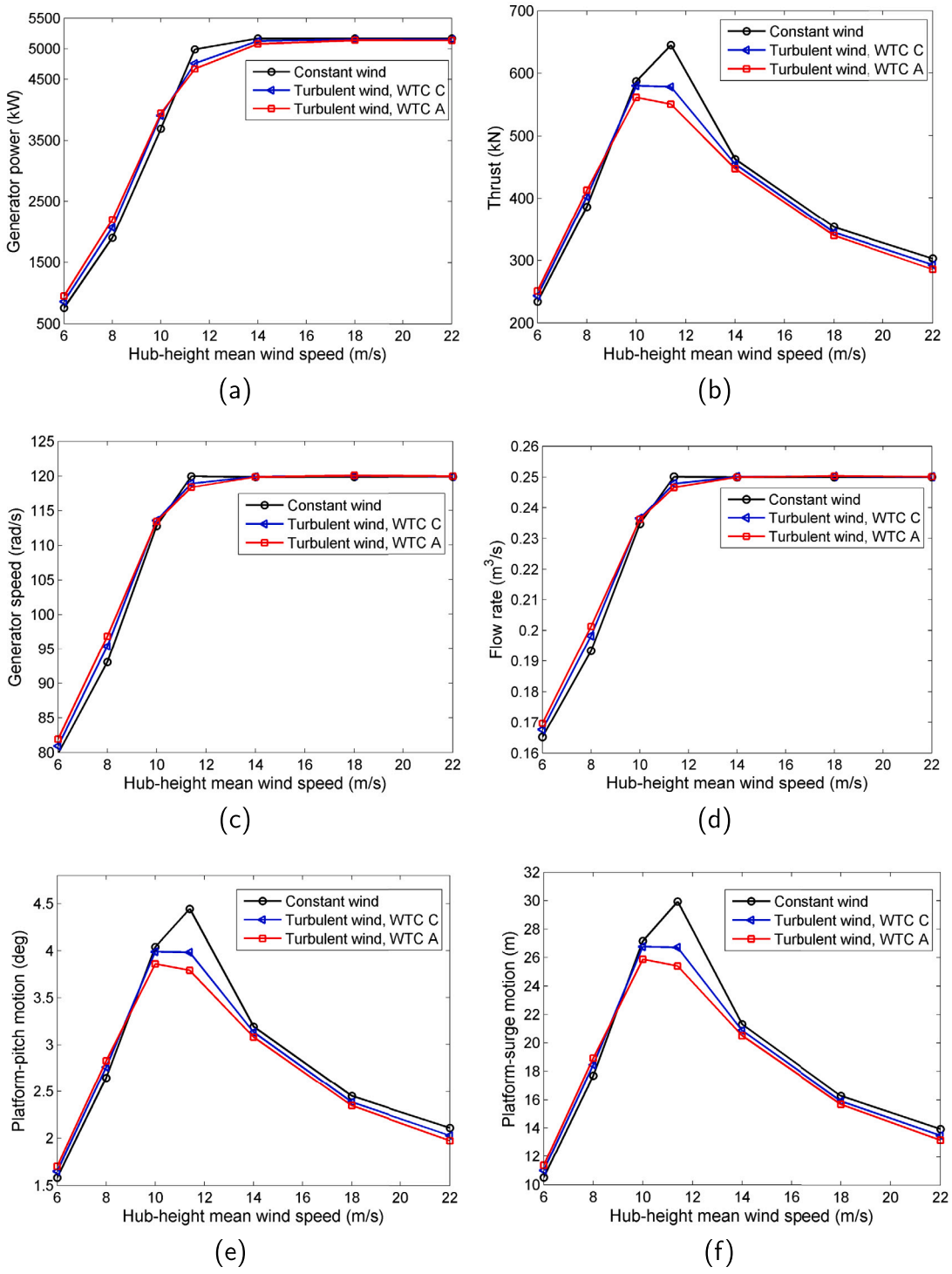

Fig. 13. Statistical means of the floating wind turbine in ECs 1–5 (each point is obtained by averaging 20 simulations): (a) generator power, (b) thrust, (c) generator speed, (d) pump flow rate, (e) platform-pitch motion, and (f) platform-surge motion.

tower top. This reduction changes the platform pitch. Similarly, in this period, the platform surge experiences a decrease in magnitude because of the blade pitch maneuver. Despite the increased oscillations in the motion response, the surge natural period can still be found.

Mean values of selected responses of the FWT under various wind and wave conditions are shown in Fig. 13. Here, we regard the mean values under constant wind conditions as the reference. Among the investigated response variables, the pump flow rate, rotor speed, and generator speed are the least affected by the wind conditions. For any wind speed, the response differences between the reference and WTC C or WTC A are below 2% and 4%, respectively. The thrust, tower-bottom bending moment, platform-pitch motion, and platform-surge motion are more affected by wind conditions, especially near the rated wind speed: under WTC A, the reductions in these variables are approximately 15%; under WTC C, the reductions are approximately 5%. At the rated wind speed, WTC A and WTC C tend to increase the mean blade pitch angle. As a result, the mean generator power is reduced by 6.5% and 4.7%, respectively.

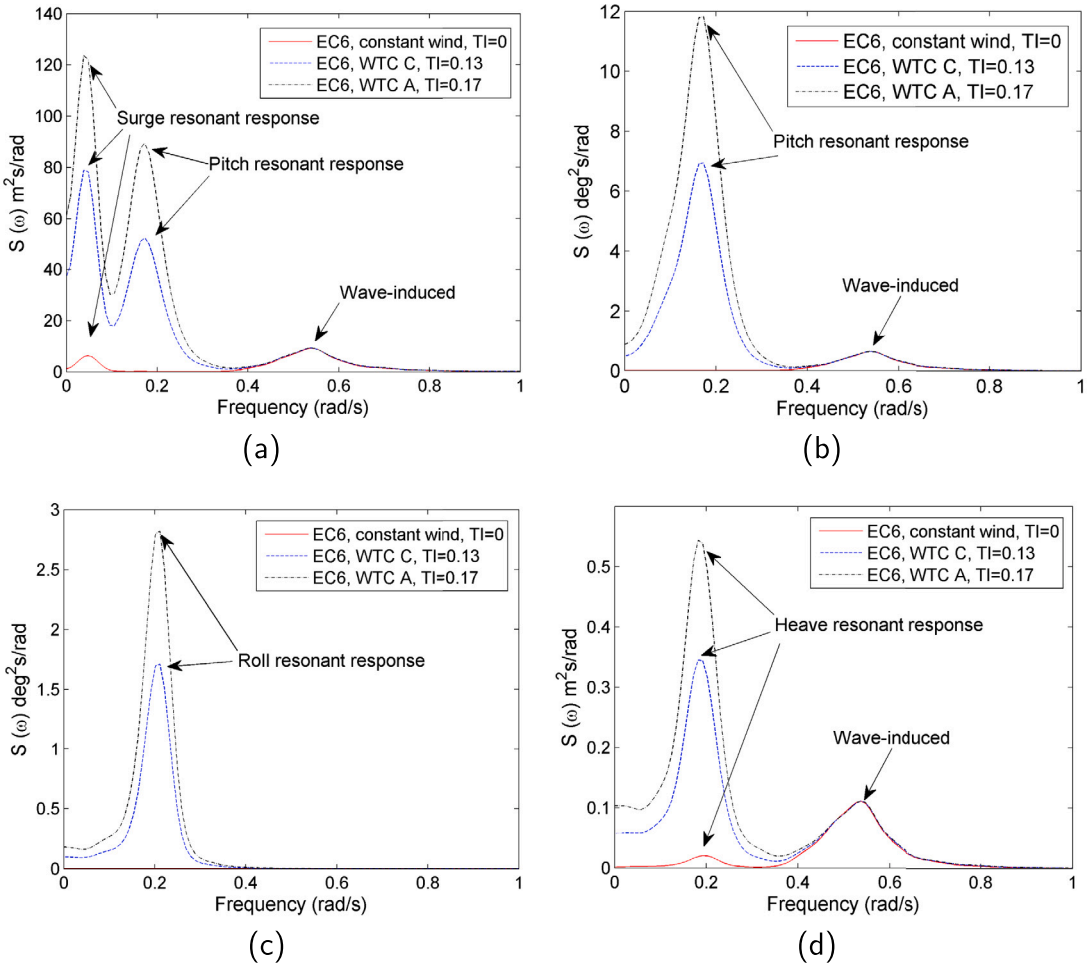

Fig. 14. Response spectra of platform motions, based on twenty 10-min simulations (EC6, U_{hub}=18 m/s, H_s=3.6 m/s, T_p=11.0 s): (a) platform-surge motion, (b) platform-pitch motion, (c) platform-roll motion, and (d) platform-heave motion.

Although turbulent wind appears to have limited impact on the mean values of the responses of the FWT, the performance of the hydraulic turbine should be further evaluated by investigating other response statistics. We summarize the results of two representative environmental conditions in Table 5. EC 2 and EC 6 correspond to the hub-height wind speeds of 8 and 18 m/s, respectively. Despite the blade-pitch control, the standard deviations of the thrust, generator speed, tower-bottom fore-aft bending moment and platform motions are larger in EC6 than in EC2. This observation may be explained by the following reasons. First, the FWT has larger wave-induced motions in EC6 than in EC2. Second, the control strategy of the spar wind turbine above the rated wind speed leads to reduced blade-pitch activity and relatively large rotor and generator speed excursions. It can be observed that the minima of the thrust, tower-bottom bending moment, and platform-pitch motion have negative values in WTC A. This observation is expected for the spar FWT, especially in those cases with larger waves and stronger turbulence. In such a case, a negative tower-bottom fore-aft bending moment may be created if the rotor experiences a decrease in thrust in the positive y direction (Fig. 6).

Using Eqs. (21)–(22), Table 6 provides a comparison of the turbines under two turbulence intensity levels. For the FWT, WTC A causes an approximately 20% increase in the standard deviations of most variables. For the LWT, the increases can exceed 30%. This reduced effect on the FWT is due to the wave loads and platform motions. The effect on most extreme responses is limited for both turbines because of operational control. For both turbines, significant relative differences in the minima of the thrust and tower-bottom bending moment exist because of the negative response values under WTC A. The absolute values of these minima are small compared to those of the maxima.

$$Rel\_diff(ECi) = \frac{Var(WTC\ A, ECi) - Var(WTC\ C, ECi)}{Var(WTC\ C, ECi)} \times 100\%\ , i = 1, 2..., 7 \tag{21}$$

$$Rel\_diff\_averg = 1/7 \sum_{i=1}^{7} Rel\_diff(ECi) \tag{22}$$

Fig. 14 shows the response spectra of the hydraulic FWT for the platform-surge, -pitch, -roll, and -heave motions under different wind conditions. Under constant wind and irregular wave conditions, the platform-pitch, -surge and -heave spectra are dominated by the wave-frequency response. Because the wind and waves are codirectional and normal to the rotor plane, the wave-induced contribution to the spectrum of the roll response is negligible. When the constant wind condition is changed to the turbulent wind condition, there are dominant contributions from the platform resonant responses in the spectra. Fig. 14(a) appears smoother than Figure 17 of [44]. This is because the spectral density function has been calculated using a Parzen window function on the estimated autocorrelation function. The effect of wind turbulence is also included in the low-frequency part. As indicated by Table 5, WTC A causes higher standard deviations than does WTC C in all responses. Accordingly, larger motion resonant peaks are associated

Table 5
Response statistics under turbulent wind and irregular wave conditions, FWT (each value based on an average of 20 simulations).

Variable	EC	Std		Max		Min	
		WTC A	WTC C	WTC A	WTC C	WTC A	WTC C
Generator power (kW)	2	774.87	595.92	4644.81	3909.40	388.26	464.76
	6	215.22	188.23	5794.37	5737.32	4395.82	4570.33
Generator torque (kN m)	2	6.51	5.31	41.73	37.44	4.39	5.19
	6	2.97	2.52	47.40	47.40	35.05	36.77
Thrust (kN)	2	103.61	82.31	735.46	663.10	172.59	204.62
	6	123.10	95.95	810.99	702.73	−13.85	63.59
Rotor speed (rad/s)	2	0.11	0.09	1.30	1.25	0.76	0.77
	6	0.10	0.08	1.55	1.50	1.00	1.05
Generator speed (rad/s)	2	8.53	6.69	115.45	110.60	79.36	81.00
	6	10.26	7.98	145.97	139.77	97.71	102.07
Blade pitch angle (deg)	2	0.08	0.01	1.04	0.22	0	0
	6	2.49	1.88	18.13	17.27	6.53	8.69
Pump flow rate (m^3/s)	2	0.021	0.018	0.257	0.246	0.150	0.152
	6	0.020	0.016	0.307	0.296	0.196	0.206
Pump pressure (bar)	2	68.02	63.85	288.71	272.78	14.06	19.40
	6	66.12	54.67	414.20	377.25	40.51	68.23
Tower-base Mx (kN m)	2	18969.4	15433.3	113086.8	100989.3	−4306.6	2836.2
	6	26789.7	22761.1	138274.3	124418.9	−38428.0	−27999.6
Platform-pitch motion (deg)	2	0.71	0.54	4.55	4.12	1.20	1.47
	6	1.21	0.94	5.66	4.97	−0.89	−0.13
Platform-surge motion (m)	2	5.01	3.87	30.01	27.12	9.38	10.83
	6	5.03	4.03	29.60	26.87	4.30	6.61

Table 6
Average relative difference (Eq. (22)) of the response statistics of the turbines between conditions WTC A and WTC C (each value based on an average of all ECs).

Variable	LWT			FWT		
	Std (%)	Max (%)	Min (%)	Std (%)	Max (%)	Min (%)
Generator power	38.26	7.54	−9.45	20.62	5.21	−9.69
Generator torque	36.06	5.94	−8.20	17.06	3.17	−7.54
Thrust	26.49	9.82	−39.03	23.46	10.03	−93.94
Rotor speed	28.36	2.17	−2.26	19.73	3.10	−3.09
Generator speed	31.35	2.30	−2.31	27.72	3.63	−3.33
Pump flow rate	27.94	2.13	−2.23	19.84	3.12	−3.23
Pump pressure	27.92	10.58	−23.41	12.88	7.28	−43.23
Tower-bottom fore-aft moment	26.73	11.25	−291.53	18.31	10.36	−37.19

with WTC A. It should be noted that, in the response spectra, the wave-induced part is not affected by wind conditions. A similar observation has been reported on a parked spar FWT [45].

For both the spar FWT and the LWT with the hydraulic transmission, statistical quantities of the power production are similar to those of the corresponding wind turbines with gear transmission. Fig. 15 demonstrates a comparison of hydraulic transmission versus gear transmission wind turbines under varying wind speeds with WTC A. Under the turbulent wind conditions, the percentage differences in the average generator power between the hydraulic and the gear transmissions is less than 2.5% for the LWT and less than 4% for the FWT. A possible cause for such differences is the time delay from aerodynamic torque to the development of pressure in the hydraulic system [13]. To improve the power generation quality of the hydraulic wind turbines, advanced blade pitch control and safety valve control can be considered.

6. Conclusions

We address the dynamic response of wind turbines with a hydraulic transmission system in this study. A utility-scale spar floating wind turbine and a land-based wind turbine are considered. The hydraulic system, expressed as ordinary differential equations, is coupled to the HAWC2 main program through an external dynamic link library. The parameters of the hydraulic pump, motor, and generator are adopted from publicly available literature. Integrated analysis of the system behavior has been performed under various wind and wave conditions. Based on the study, the following conclusions can be made:

- With the current hydraulic system, both the spar floating wind turbine and the land-based wind turbine have decent performances under various environmental conditions. The dynamic response results show that the power performance of the hydraulic turbines is similar to that of conventional wind turbines with gear transmission.
- For the land-based wind turbine, the hydraulic system provides a torque that balances the external aerodynamic torque under constant wind conditions, and all response variables reach a steady state. Turbulent wind conditions have small effects on the response mean values: the generator power and thrust are most affected near the rated wind speed, whereas the generator speed and pump flow rate are not. Stronger turbulence is associated with larger response standard deviations, which may exceed 30% in Wind Turbine Class A. Because of the blade pitch control, the response standard deviations are reduced above the rated wind speed compared to below the rated wind speed.
- For the spar floating wind turbine and under constant wind conditions, wave forces create platform motions and affect the incoming wind on the rotor. Consequently, the floating wind turbine does not exhibit steady-state responses, and the fluctuations in the responses tend to increase in larger waves. Turbulence has limited impact on the response mean values of the floating wind

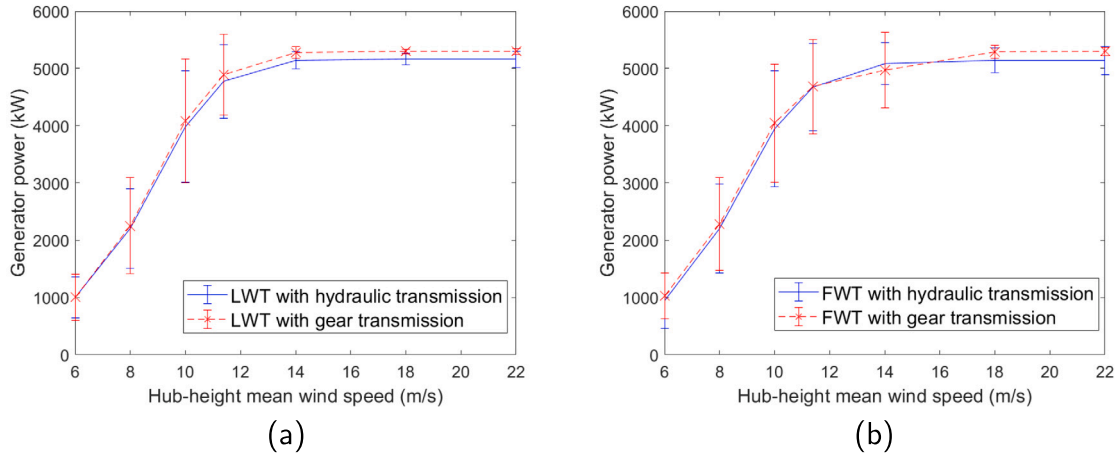

Fig. 15. Comparison of generator power between hydraulic and gear transmissions under WTC A: (a) land-based wind turbine (b) spar floating wind turbine; each mean and standard deviation is obtained based on an average of 20 simulations.

turbine, but a higher turbulence level causes greater standard deviations in the responses. These observations correspond well with the land-based wind turbine, although a reduced effect of turbulence on the response standard deviations exists for the floating wind turbine. In contrast to the land-based wind turbine, the spar floating wind turbine could have higher standard deviations above the rated wind speed. The resonant parts in the motion response spectra of the floating platform are also sensitive to wind conditions.

7. Future work

The present study focuses on the feasibility of simulating wind turbines with hydraulic systems under operational conditions. Further work is needed to optimize the wind turbine structure and to assess the lifecycle costs of the hydraulic wind energy systems. The assumptions of laminar flow and rigid pipelines are made when the pipeline dynamics is modeled. In reality, the pipelines can have flexibility and more complicated structural dynamics and reliability issues can arise during motions of a floating wind turbine. These issues can be addressed in future.

CRediT authorship contribution statement

Zhiyu Jiang: Numerical simulations, Methodology, Writing. **Limin Yang:** Concept contruction, Theoretical development, Methodology, Results discussion, Writing. **Zhen Gao:** Concept contruction, Methodology, Results discussion, Critical review. **Torgeir Moan:** Concept contruction, Methodology, Results discussion, Critical review.

Declaration of competing interest

The authors declare that they have no known competing financial interests or personal relationships that could have appeared to influence the work reported in this paper.

Data availability

Data will be made available on request.

References

[1] A. Ragheb, M. Ragheb, Wind turbine gearbox technologies, in: Proceedings of the 1st International Nuclear and Renewable Energy Conference, INREC10, Amman, Jordan, March 21-24, 2010.

[2] W. Musial, S. Butterfield, B. McNiff, Improving wind turbine gearbox reliability, in: Proceedings of the European Wind Energy Conference, Milan, Italy, May 2007.

[3] E. de Vries, The evolution of wind turbine drive systems, 2014, www.windpowermonthly.com.

[4] S. Watson, A. Moro, V. Reis, C. Baniotopoulos, S. Barth, G. Bartoli, F. Bauer, E. Boelman, D. Bosse, A. Cherubini, et al., Future emerging technologies in the wind power sector: A European perspective, Renew. Sustain. Energy Rev. 113 (2019) 109270.

[5] S. Salter, M. Rea, Hydraulics for wind, in: Proceedings of the European Wind Energy Conference in Hamburg in October, 1984.

[6] J. Cruz, Ocean Wave Energy Current Status and Future Prespectives, Green Energy and Technology, Springer-Verlag Berlin Heidelberg, 2008.

[7] L. Yang, J. Hals, T. Moan, Analysis of dynamic effects relevant for the wear damage in hydraulic machines for wave energy conversion, Ocean Eng. 37 (13) (2010) 1089–1102.

[8] S. Rybak, Description of the 3 MW SWT-3 wind turbine at San Gorgonio Pass California, in: The Bendix Corporation Energy, Environmental and Technology Office, 1981.

[9] N. Diepeveen, On the Application of Fluid Power Transmission in Offshore Wind Turbines (Ph.D. thesis), Delft University of Technology, Delft, the Netherlands, 2013.

[10] J. Schmitz, N. Vatheuer, H. Murrenhoff, Development of a hydrostatic transmission for wind turbines, in: The 7th International Fluid Power Conference, 2010.

[11] P. Chapple, O. Dahlhaug, P. Haarberg, Patent WO 2007/083036 A1: A turbine driven electric power production system and a method for control thereof, 2011.

[12] A.J. Laguna, Steady-State Performance of the Delft Offshore Turbine (Ph.D. thesis), Delft University of Technology, Delft, the Netherlands, 2010.

[13] B. Skaare, B. Hornsten, F.G. Nielsen, Modeling, simulation and control of a wind turbine with a hydraulic transmission system, Wind Energy 16 (2012) 1259–1276.

[14] M. Sasaki, A. Yuge, T. Hayashi, T. Nishino, M. Uchida, T. Noguchi, Large capacity hydrostatic transmission with variable displacement, in: The 9th International Fluid Power Conference IFK, March 24-26, Aachen, Germany, 2014.

[15] F. Wang, J. Chen, B. Xu, K.A. Stelson, Improving the reliability and energy production of large wind turbine with a digital hydrostatic drivetrain, Appl. Energy 251 (2019) 113309.

[16] L. Yang, Z. Jiang, Z. Gao, T. Moan, Dynamic analysis of a floating wind turbine with a hydraulic transmission system, in: The Twenty-Fifth International Ocean and Polar Engineering Conference, 2015.

[17] Z. Ren, A.S. Verma, Y. Li, J.J. Teuwen, Z. Jiang, Offshore wind turbine operations and maintenance: A state-of-the-art review, Renew. Sustain. Energy Rev. 144 (2021) 110886.

[18] W. Chen, X. Wang, F. Zhang, H. Liu, Y. Lin, Review of the application of hydraulic technology in wind turbine, Wind Energy 23 (7) (2020) 1495–1522.

[19] W. Chen, F. Gao, X. Meng, A. Ren, S. Zhou, An offshore hydraulic wind turbine generator with variable-diameter rotor: Design, modeling and experiment, Proc. Inst. Mech. Eng. Part M: J. Eng. Marit. Environ. 231 (2) (2017) 521–532.

[20] Z. Jiang, Installation of offshore wind turbines: A technical review, Renew. Sustain. Energy Rev. 139 (2021) 110576.

[21] B. Skaare, F.G. Nielsen, T.D. Hanson, R. Yttervik, O. Havmøller, A. Rekdal, Analysis of measurements and simulations from the Hywind Demo floating wind turbine, Wind Energy 18 (6) (2015) 1105–1122.

[22] Equinor ASA, Hywind Tampen, 2022, https://www.equinor.com/energy/hywind-tampen 20122 (Accessed May 2022).
[23] International Electrotechnical Commmission, IEC 61400–1 Wind Turbine Part 1: Design Requirements, third ed., 2007.
[24] International Electrotechnical Commission, IEC 61400-3 Wind Turbines. Part 3: Design Requirements for offshore wind turbines, third ed., 2009.
[25] M. Karimirad, T. Moan, Extreme dynamic structural response analysis of catenary moored spar wind turbine in harsh environmental conditions, J. Offshore Mech. Arct. Eng. 133 (4) (2011) 0411031–04110314.
[26] Z. Jiang, M. Karimirad, T. Moan, Dynamic response analysis of wind turbines under blade pitch system fault, grid loss, and shutdown events, Wind Energy (2013) http://dx.doi.org/10.1002/We.1639.
[27] T.J. Larsen, How 2 HAWC2, The User's Manual, Technical Report, Risø National Laboratory, Technical University of Denmark, Roskilde, Denmark, 2009.
[28] J. Jonkman, FAST User's Guide, Technical Report, National Renewable Energy Laboratory, Golden, CO, USA, 2009.
[29] E. Bossanyi, GH Bladed Version 3.51 User Manual, Technical Report, Garrad Hassan and Partners Ltd, 2003.
[30] L. Yang, T. Moan, Dynamic analysis of wave energy converter by incorporating the effect of hydraulic transmission lines, Ocean Eng. 38 (16) (2011) 1849–1860.
[31] Z. Jiang, L. Yang, Z. Gao, T. Moan, Numerical simulation of a wind turbine with a hydraulic transmission system, Energy Procedia 53 (2014) 44–55.
[32] E. Fehlberg, Classical fourth-and lower order Runge-Kutta formulas with stepsize control and their application to heat transfer problems, Technical Report, National Aeronautics and Space Administration, Marshall Space Flight Center, Marshall, AL, USA, 1970.
[33] Bosch Rexroth AG, www.boschrexroth.com 2014.
[34] O. Egeland, J.T. Gravdahl, Modeling and simulation for automatic control, Marine Cybernetics (2002) Trondheim, Norway.
[35] L. Yang, J. Hals, T. Moan, Comparative study of bond graph models for hydraulic transmission lines with transient flow dynamics, J. Dyn. Syst. Meas. Control 134 (3) (2012).
[36] L. Yang, T. Moan, Bond graph representations of hydraulic pipelines using normal modes with dissipative friction, Simulation 89 (2) (2013) 199–212.
[37] J. Jonkman, Definition of a 5-MW Reference Wind Trubine for Offshore System Development, Technical Report, National Renewable Energy Laboratory, Golden, CO, USA, 2009.
[38] J. Jonkman, Definition of the Floating System for Phase IV of OC3, Technical Report, National Renewable Energy Laboratory, Golden, CO, USA, 2010.
[39] T.J. Larsen, T.D. Hanson, A method to avoid negative damped low frequent tower vibrations for a floating, pitch controlled wind turbine, in: J. Phys. Conf. Ser., 75 (1) (2007) 012073.
[40] J. Morison, J. Johnson, S. Schaaf, The force exerted by surface waves on piles, J. Pet. Technol. 2 (05) (1950) 149–154.
[41] M. Karimirad, Q. Meissonnier, Z. Gao, T. Moan, Hydroelastic code-to-code comparison for a tension leg spar-type floating wind turbine, Mar. Struct. 24 (4) (2011) 412–435.
[42] L. Shampine, H. Watts, The art of writing a Runge-Kutta code II, Appl. Math. Comput. 5 (2) (1979) 93–121.
[43] L. Li, Z. Gao, T. Moan, Joint distribution of environmental condition at five european offshore sites for design of combined wind and wave energy devices, J. Offshore Mech. Arct. Eng. 137 (3) (2015).
[44] L. Li, Y. Liu, Z. Yuan, Y. Gao, Wind field effect on the power generation and aerodynamic performance of offshore floating wind turbines, Energy 157 (2018) 379–390.
[45] Z. Jiang, M. Karimirad, T. Moan, Response analysis of parked spar-type wind turbine considering blade-pitch mechanism fault, Int. J. Offs. Polar Eng. 23 (02) (2013).